

Cluster size distributions of discrete random fields

Dan Cheng and John Ginos

Arizona State University

Abstract

We study discrete random fields $\{X_t : t \in \mathbb{Z}^d\}$ parameterized on the d -dimensional integer lattice \mathbb{Z}^d . For a fixed threshold u , the excursion set $\{t \in \mathbb{Z}^d : X_t > u\}$ decomposes into connected components or clusters, whose size, defined as the number of lattice points they contain, are random. This paper investigates the probability distribution of these cluster sizes. For stationary random fields, we derive exact expressions for the cluster size distribution. To address nonstationary settings, we introduce a peak-based cluster size distribution, which characterizes the distribution of cluster sizes conditional on the presence of a local maximum above u . This formulation provides a tractable alternative when exact cluster size distributions are analytically inaccessible. The proposed framework applies broadly to Gaussian and non-Gaussian random fields, relying only on their joint dependence structure. Our results provide a theoretical foundation for quantifying spatial extent in discretely sampled data, with applications to medical imaging, geoscience, environmental monitoring, and other scientific areas where thresholded random fields naturally arise.

Keywords: random fields; discrete lattice; spatial extent; connected components; cluster size; peak-based; stationary; nonstationary; threshold.

Mathematics Subject Classification: 62M40, 62G32, 62E15, 60G70, 60G60.

1 Introduction

Random fields play a central role in modern spatial statistics, stochastic modeling, and signal detection. They provide a natural framework for characterizing spatially correlated data across a wide range of scientific disciplines, including medical imaging, geoscience, environmental studies, and cosmology [2, 5, 9, 16, 19, 24]. When a random field is observed over a discrete lattice such as \mathbb{Z}^d , the resulting process is referred to as a *discrete random field*. A fundamental problem in the analysis of such fields concerns the geometric and topological properties of regions where the field exceeds a fixed threshold level u . These regions, commonly called excursion sets, decompose into random connected components, or clusters, formed by neighboring lattice sites above the threshold.

Understanding the statistical distribution of cluster sizes in random fields is fundamental for both theory and applications. In spatial statistics and random field theory, the cluster size

distribution under a null (pure noise) model provides a benchmark for assessing the significance of observed spatial patterns. For example, in neuroimaging, random field theory underlies cluster-based inference procedures for detecting activation regions in fMRI data [3, 10, 14, 16, 20, 23, 25]. Similar principles arise in geoscience and cosmology, where cluster size distributions describe the spatial extent of anomalies in correlated data [1, 4, 9, 18, 21]. Recent work in climate and environmental statistics has emphasized the importance of spatial extent inference, which aims to quantify the areal footprint of extreme events [22, 26]. In parallel, inference for threshold exceedances in random fields has been applied to spatiotemporal extreme value analysis [15, 17].

While the geometry of excursion sets for continuous Gaussian fields has been extensively studied through tools such as the Gaussian kinematic formula and Euler characteristic heuristics [2, 24], exact cluster-size distributions are typically intractable in continuous settings. In contrast, for discrete random fields on lattices, it is possible to formulate and compute cluster size distributions explicitly under suitable assumptions. The discrete setup allows a combinatorial characterization of connected components, leading to exact expressions in low dimensions and numerically tractable formulations in higher dimensions.

In this paper, we investigate the cluster size distribution of discrete stationary random fields $\{X_t : t \in \mathbb{Z}^d\}$ defined on the d -dimensional integer lattice \mathbb{Z}^d . We focus on the probabilistic structure of clusters that arise arising from thresholding the field at a fixed level $u \in \mathbb{R}$. Clusters are defined as connected components of the excursion set $\{t \in \mathbb{Z}^d : X_t > u\}$. Each cluster above the threshold u , denoted by C_u , has a random size $|C_u|$, defined simply as the number of lattice points in the component. Illustrations in one and two dimensions are provided in Figures 1 and 3. Our first objective is to derive the *exact cluster size distribution*

$$\mathbb{P}(|C_u| = k \mid \text{a cluster } C_u \text{ above } u \text{ exists}), \quad k = 1, 2, \dots,$$

for stationary random fields, where the covariance structure depends only on spatial lag.

Motivated by recent advances in peak inference for random fields [6, 7, 8] and peaks-over-threshold methods [15, 17], we further introduce and develop the *peak-based cluster size distribution*. This characterizes the distribution of cluster sizes conditional on the presence of a local maximum above u . Specifically, we derive the conditional probability

$$\mathbb{P}(|C_u(t)| = k \mid t \text{ is a local maximum and } X_t > u), \quad k = 1, 2, \dots,$$

where $C_u(t)$ denotes the cluster containing an observed local maximum t that exceeds the threshold u . This formulation connects local peak statistics with cluster extent, bridging ideas from spatial extreme value theory and classical random field analysis. It is particularly valuable in nonstationary settings, where local variations in the covariance structure influence both the shape and spatial extent of clusters. In contrast, obtaining exact cluster size distributions in the nonstationary case appears analytically intractable.

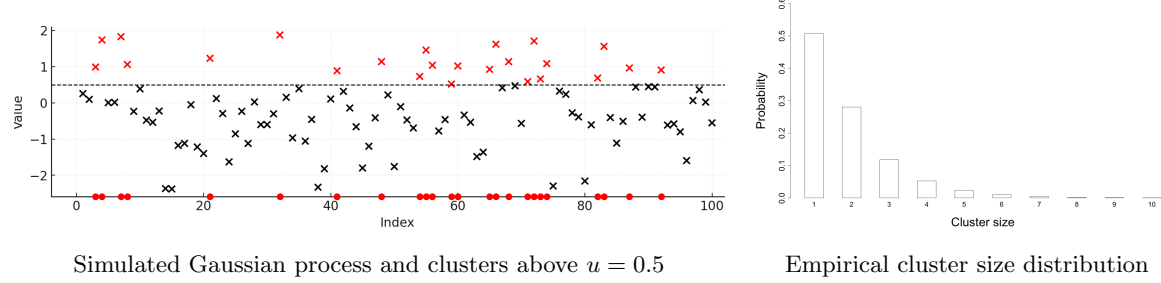


Figure 1: The left panel is the scatter plot of a simulated realization of a centered stationary Gaussian process with covariance $C(t, s) = e^{-(t-s)^2}$, where exceedances above the threshold $u = 0.5$ are marked in red, and the corresponding clusters are marked in consecutive red dots along the index \mathbb{Z} . This realization exhibits 14 observed clusters: 7 of size one, 5 of size two, 1 of size three, and 1 of size four. The right panel displays the empirical cluster size distribution obtained from repeated simulations.

In many applications, data are observed on discrete grids rather than as continuous fields. The framework developed in this paper thus provides a unified theoretical foundation for cluster modeling and inference in discrete random fields. Beyond its intrinsic theoretical interest, the results have broad practical implications for signal detection and spatial extent inference in correlated lattice data. Applications include neuroimaging [3, 10, 14, 16, 23], geophysical anomaly detection [9, 21], and climate data analysis [11, 13], where discretely sampled random fields are ubiquitous.

Finally, while Gaussian random fields serve as a convenient and widely used reference model, the general framework developed here does not require Gaussianity. As will become clear from the arguments below, the derivations depend only on the joint dependence structure of the field. Consequently, the methodology applies to broad classes of non-Gaussian random fields, provided their finite-dimensional distributions are well defined.

2 The exact cluster size distribution

We begin with stationary discrete random fields and derive exact expressions for their cluster size distributions. In general, the analysis of random fields indexed by \mathbb{Z}^d is conceptually rich and technically demanding. To present the main ideas in a transparent manner, we first focus on the one-dimensional case, where the structure of clusters and the required joint probabilities admit explicit characterization.

2.1 Stationary processes on \mathbb{Z}

Let $\{X_t : t \in \mathbb{Z}\}$ be a real-valued centered stationary process on the one-dimensional integer lattice \mathbb{Z} . Fix a threshold $u \in \mathbb{R}$ and consider the excursion set

$$\{t \in \mathbb{Z} : X_t > u\}.$$

Its connected components (intervals of consecutive integers) are called *clusters*. The size of a cluster is defined as the number of lattice points it contains. We denote the size of a cluster by S_u and study the distribution

$$\mathbb{P}(S_u = k), \quad k = 1, 2, \dots,$$

which is interpreted as the probability that a cluster above level u has size k , conditional on the event that such a cluster exists. Formally,

$$\mathbb{P}(S_u = k) = \mathbb{P}(|C_u| = k \mid \text{a cluster } C_u \text{ above } u \text{ exists}), \quad (2.1)$$

where $|C_u|$ denotes the size of a cluster C_u . Figure 1 provides a visual illustration. The following theorem gives an exact closed-form expression for this cluster size distribution.

Theorem 2.1. *Let $\{X_t : t \in \mathbb{Z}\}$ be a centered stationary process and let $u \in \mathbb{R}$ be a fixed threshold. Then, for $k = 1, 2, \dots$,*

$$\mathbb{P}(S_u = k) = \frac{\mathbb{P}(X_{-1} \leq u, X_0 > u, X_1 > u, \dots, X_{k-1} > u, X_k \leq u)}{\mathbb{P}(X_{-1} \leq u, X_0 > u)}. \quad (2.2)$$

Proof. By stationarity, the size distribution of clusters is invariant under translations of the index set. Hence, it suffices to study clusters whose leftmost point is at the origin. The event that a cluster above u starts at 0 is exactly $\{X_{-1} \leq u, X_0 > u\}$.

Thus, the cluster size distribution can be expressed as the conditional probability

$$\begin{aligned} \mathbb{P}(S_u = k) &= \mathbb{P}(|C_u| = k \mid \text{there exists a cluster } C_u \text{ above } u \text{ starting at 0}) \\ &= \mathbb{P}(|C_u| = k \mid X_{-1} \leq u, X_0 > u), \quad k = 1, 2, \dots \end{aligned}$$

Under this conditioning, the size of the cluster is the number of consecutive exceedances starting at 0 before the process falls back below u . Hence the cluster C_u has size k if and only if

$$X_1 > u, \dots, X_{k-1} > u, X_k \leq u.$$

Formula (2.2) follows directly from the conditional probability rule. \square

Example 2.2 Let X_t , $t \in \mathbb{Z}$, be a white noise process with common cumulative distribution function (CDF) F . Let $p = F(u)$ and $q = 1 - p$. Then, by (2.2),

$$\mathbb{P}(S_u = k) = \frac{p^2 q^k}{pq} = pq^{k-1}, \quad k = 1, 2, \dots. \quad (2.3)$$

Thus, in the one-dimensional i.i.d. case, the cluster size has a geometric distribution. \square

2.2 An alternative perspective via the empirical distribution

We next demonstrate that Theorem 2.1 is consistent with the empirical cluster size distribution computed in simulations. Before doing so, we introduce an equivalent interpretation of the cluster size distribution that is particularly convenient for connecting theory with empirical estimation.

In one dimension, each cluster above u is an interval of consecutive indices. By stationarity, all such clusters are statistically equivalent up to translation. We therefore designate the *root* of a cluster as its leftmost point and translate so that this root is at the origin. A size- k cluster then has the canonical index set $\{0, 1, \dots, k-1\}$.

Let w_k denote the probability that there exists a size- k cluster above u with root at 0, i.e.,

$$\begin{aligned} w_k &= \mathbb{P}(\text{there exists a size-}k \text{ cluster above } u \text{ starting at 0}) \\ &= \mathbb{P}(X_{-1} \leq u, X_0 > u, X_1 > u, \dots, X_{k-1} > u, X_k \leq u). \end{aligned} \quad (2.4)$$

The quantity w_k represents the *per-lattice density* of size- k clusters. Consequently, in a domain of size N , the expected number of size- k clusters above u is Nw_k .

Summing w_k over all over all possible sizes $k \geq 1$ yields the probability that there exists a cluster above u with root at 0:

$$\sum_{k=1}^{\infty} w_k = \mathbb{P}(\text{there exists a cluster above } u \text{ starting at 0}) = \mathbb{P}(X_{-1} \leq u, X_0 > u). \quad (2.5)$$

Thus, $\sum_{k \geq 1} w_k$ represents the per-lattice density of all clusters above u , and the expected number of clusters above u in a domain of size N is $N \sum_{k \geq 1} w_k$.

Substituting (2.4) and (2.5) into the definition of cluster size distribution (2.1), and using stationarity, we recover the expression in (2.2):

$$\mathbb{P}(S_u = k) = \frac{w_k}{\sum_{j=1}^{\infty} w_j}.$$

We now connect this to the empirical distribution used in simulations. Suppose the observation window consists of N lattice sites. For $k \geq 1$, the empirical probability mass function of the cluster size is given by

$$\begin{aligned} \frac{\#\{\text{size-}k \text{ clusters above } u\}}{\#\{\text{all clusters above } u\}} &= \frac{\#\{\text{size-}k \text{ clusters above } u\}/N}{\#\{\text{all clusters above } u\}/N} \\ &\xrightarrow{\text{a.s.}} \frac{\text{average number of size-}k \text{ clusters per lattice site}}{\text{average number of clusters per lattice site}} \\ &= \frac{w_k}{\sum_{j=1}^{\infty} w_j}, \quad \text{as } N \rightarrow \infty, \end{aligned} \quad (2.6)$$

where the convergence follows from the strong law of large numbers under stationarity and ergodicity. Intuitively, as the observation window grows, the empirical relative frequencies of cluster sizes converge to the theoretical cluster size distribution.

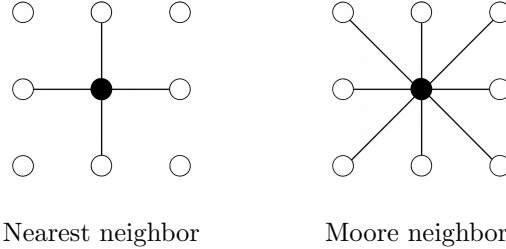


Figure 2: Two neighbourhood systems in \mathbb{Z}^2 . Left: nearest neighbor connectivity as in (2.7), where each point has 4 neighbors. Right: Moore neighbor connectivity as in (2.8), where each point has 8 neighbors (including diagonals).

2.3 Stationary random fields on \mathbb{Z}^d

We now extend the analysis to a stationary random field on \mathbb{Z}^d . In higher dimensions, issues that were trivial in one dimension, such as the possible shapes of clusters and the ordering of points, require additional care.

2.3.1 Basic notation

Let $\{X_t : t \in \mathbb{Z}^d\}$ be a centered stationary random field indexed on the d -dimensional integer lattice \mathbb{Z}^d . Clusters are defined as connected components of the excursion set $\{t \in \mathbb{Z}^d : X_t > u\}$. To define connectivity we introduce two neighbourhood systems on \mathbb{Z}^d .

Denote the origin by $o = (0, \dots, 0)$, and let $e_1 = (1, 0, \dots, 0), \dots, e_d = (0, 0, \dots, 1)$ be the standard basis of \mathbb{R}^d . For $t = (t_1, t_2, \dots, t_d) \in \mathbb{Z}^d$, we define the *nearest neighbor* set of t by

$$\{t' \in \mathbb{Z}^d : \|t' - t\| = 1\} = \{t \pm e_i : i = 1, \dots, d\}, \quad (2.7)$$

where $\|\cdot\|$ denotes the Euclidean norm. Under nearest neighbor connectivity each site has exactly $2d$ neighbors.

For completeness, we also introduce the *Moore neighbor* set of t :

$$\{t' \in \mathbb{Z}^d : \|t' - t\|_\infty = 1\}, \quad (2.8)$$

where $\|(t_1, \dots, t_d)\|_\infty = \max_{1 \leq i \leq d} |t_i|$ denotes the maximum norm. Thus, the Moore neighbor includes also diagonals and contains $3^d - 1$ points. Figure 2 illustrates these two neighborhood systems for $d = 2$.

We generalize the one-dimensional approach by defining a canonical root for each cluster. In \mathbb{Z}^d , each cluster above u is a finite connected set of indices (connected under either the nearest or the Moore neighborhood). As in one dimension, stationarity suggests choosing the “lower left” point of the cluster as its root.

To make this precise, we introduce the *lexicographic order* on \mathbb{Z}^d . For two distinct points $t = (t_1, t_2, \dots, t_d)$ and $t' = (t'_1, t'_2, \dots, t'_d)$ in \mathbb{Z}^d , we write

$$t <_{\text{lex}} t' \text{ if and only if there exists } j \text{ such that } t_j < t'_j \text{ and } t_i = t'_i \text{ for all } i < j.$$

Thus the first coordinate where the two vectors differ determines the ordering. For example, in \mathbb{Z}^2 ,

$$(0, 0) <_{\text{lex}} (0, 1) <_{\text{lex}} (1, -1) <_{\text{lex}} (1, 0) <_{\text{lex}} (1, 1).$$

This is a total order, so every finite nonempty subset of \mathbb{Z}^d has a unique smallest element. We define the *root* of a cluster to be this lexicographically smallest element. By stationarity, we may translate a cluster so that its root is at the origin o ; in particular, $o <_{\text{lex}} t$ for all nonzero t in the cluster.

Figure 3 provides examples of clusters and empirical cluster size histograms for an isotropic Gaussian field on \mathbb{Z}^2 under both nearest and Moore neighbors. Since Moore neighbors include also diagonals as connected sites, larger clusters are observed more frequently than under nearest-neighbor connectivity. The same phenomenon arises when moving from one to two dimensions (see Figures 1 and 3), as the increased number of connections similarly promotes the formation of larger connected components.

2.3.2 Cluster size distribution in \mathbb{Z}^d

For $k = 1, 2, \dots$, denote the collection of all rooted clusters of size k by

$$\mathcal{C}_k^{\text{root}} = \{\text{size-}k \text{ clusters above } u \text{ with the root at } o\}.$$

For example, under nearest neighbors in \mathbb{Z}^2 ,

$$\begin{aligned} \mathcal{C}_1^{\text{root}} &= \{o\}, & \mathcal{C}_2^{\text{root}} &= \{\{o, e_1\}, \{o, e_2\}\}, \\ \mathcal{C}_3^{\text{root}} &= \{\{o, e_1, 2e_1\}, \{o, e_1, (1, 1)\}, \{o, e_1, (1, -1)\}, \{o, e_1, e_2\}, \{o, e_2, 2e_2\}, \{o, e_2, (1, 1)\}\}. \end{aligned} \tag{2.9}$$

If one uses Moore neighbors, then $\mathcal{C}_2^{\text{root}}$ contains two additional sets $\{o, (1, 1)\}$ and $\{o, (1, -1)\}$, and $\mathcal{C}_3^{\text{root}}$ includes further shapes such as $\{o, (1, 1), (2, 2)\}$, $\{o, e_1, (2, 1)\}$, and others.

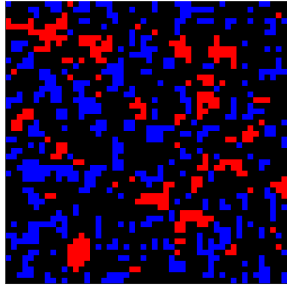
For a finite set $D \subset \mathbb{Z}^d$, we write $X_D > u$ if $X_t > u$ for all $t \in D$, and $X_D \leq u$ if $X_t \leq u$ for all $t \in D$. Let $\mathcal{N}(D)$ denote the *exterior neighbor* set of D :

$$\mathcal{N}(D) = \begin{cases} \{t' \in \mathbb{Z}^d \setminus D : \|t' - t\| = 1 \text{ for some } t \in D\}, & \text{nearest neighbors,} \\ \{t' \in \mathbb{Z}^d \setminus D : \|t' - t\|_\infty = 1 \text{ for some } t \in D\}, & \text{Moore neighbors.} \end{cases} \tag{2.10}$$

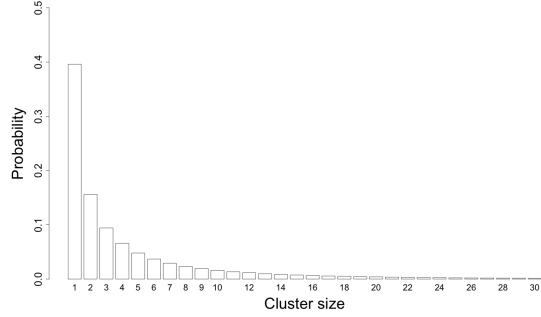
We can now state the exact cluster size distribution in \mathbb{Z}^d .

Theorem 2.3. *Let $\{X_t : t \in \mathbb{Z}^d\}$ be a centered stationary random field and let $u \in \mathbb{R}$ be a fixed threshold. Then, for $k = 1, 2, \dots$,*

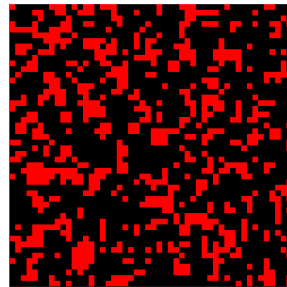
$$\mathbb{P}(S_u = k) = \frac{w_k}{\sum_{j=1}^{\infty} w_j}, \tag{2.11}$$



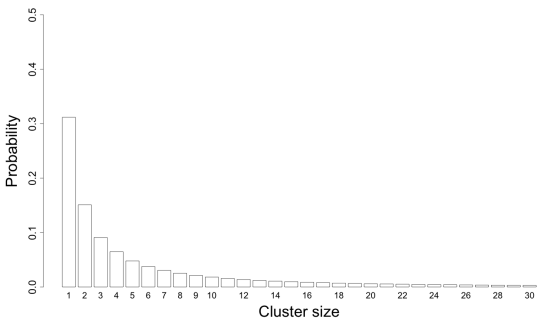
(a) Clusters (nearest neighbor)



(b) Empirical cluster size distribution (nearest neighbor)



(c) Clusters (Moore neighbor)



(d) Empirical cluster size distribution (Moore neighbor)

Figure 3: Simulation of clusters and empirical cluster size distributions for an isotropic Gaussian field on \mathbb{Z}^2 with covariance $C(t, s) = e^{-\|t-s\|^2}$ and threshold $u = 0.5$. Panels (a) and (b) use the nearest neighbors, while panels (c) and (d) use Moore neighbors. In (a), distinct clusters above u are highlighted in blue and red (note that diagonal sites are not connected under nearest neighbors); while in (c), they are marked in red. Panels (b) and (d) display the corresponding empirical cluster size distributions from repeated simulations.

where w_k is the probability that a cluster with root at the origin has size k , i.e.,

$$w_k = \sum_{D \in \mathcal{C}_k^{\text{root}}} \mathbb{P}(X_D > u, X_{\mathcal{N}(D)} \leq u). \quad (2.12)$$

Proof. By stationarity we may assume that the cluster under consideration, denoted C_u , has root at the origin o . Equivalently, we condition on the event that o is the lexicographically smallest point in its cluster. Then

$$\begin{aligned} \mathbb{P}(S_u = k) &= \mathbb{P}(|C_u| = k \mid \text{there exists a cluster } C_u \text{ above } u \text{ with root at } o) \\ &= \frac{\mathbb{P}(C_u \text{ with root at } o \text{ has size } k)}{\mathbb{P}(\text{there exists a cluster above } u \text{ with root at } o)}. \end{aligned}$$

The numerator is obtained by summing over all rooted clusters of size k :

$$\mathbb{P}(C_u \text{ with root at } o \text{ has size } k) = \sum_{D \in \mathcal{C}_k^{\text{root}}} \mathbb{P}(X_D > u, X_{\mathcal{N}(D)} \leq u) = w_k;$$

and similarly, the denominator becomes

$$\sum_{j=1}^{\infty} \sum_{D \in \mathcal{C}_j^{\text{root}}} \mathbb{P}(X_D > u, X_{\mathcal{N}(D)} \leq u) = \sum_{j=1}^{\infty} w_j.$$

Substituting these into the conditional probability formula yields (2.11). \square

Example 2.4 Let X_t , $t \in \mathbb{Z}^2$, be a two-dimensional white noise field with common CDF F . Let $p = F(u)$ and $q = 1 - p$. Inspecting the sets in $\mathcal{C}_k^{\text{root}}$ (e.g., (2.9)) and the corresponding boundary sizes $|\mathcal{N}(D)|$ yields that, under nearest neighbors,

$$w_1 = p^4 q, \quad w_2 = 2p^6 q^2, \quad w_3 = (2p^8 + 4p^7)q^3.$$

Similarly, under Moore neighbors,

$$w_1 = p^8 q, \quad w_2 = (2p^{10} + 2p^{12})q^2, \quad w_3 = (6p^{12} + 8p^{14} + 4p^{15} + 2p^{16})q^3.$$

In general, the combinatorial complexity of $\mathcal{C}_k^{\text{root}}$ grows rapidly with k , so closed-form expressions for w_k are rarely available. Nevertheless, w_k can be evaluated numerically by enumerating shapes or approximated via Monte-Carlo simulation. \square

Remark 2.5 [Interpretation of w_k and empirical relations.] Each w_k is the per-lattice density of size- k clusters. If the field is observed on a finite domain of N^d lattice points, then the expected numbers of size- k clusters and of all clusters above u are $N^d w_k$ and $N^d \sum_{j \geq 1} w_j$, respectively. Consequently, the empirical proportion of size- k clusters among all observed clusters converges to $w_k / \sum_{j \geq 1} w_j$ under stationarity and ergodicity, in direct analogy with (2.6) in the one-dimensional case. Moreover,

$$\hat{w}_k = \frac{\#\{\text{size-}k \text{ clusters above } u\}}{N^d} \quad \text{and} \quad \sum_{j=1}^{\infty} \hat{w}_j = \frac{\#\{\text{all clusters above } u\}}{N^d}, \quad (2.13)$$

are natural empirical estimators of w_k and $\sum_{j \geq 1} w_j$, respectively. \square

Remark 2.6 [Computation of w_k .] For large k , the probabilities w_k in (2.12) are difficult to compute analytically, and the denominator $\sum_{j \geq 1} w_j$ in (2.11) is rarely available in closed form. Section 2.3.4 below describes Monte-Carlo estimators for w_k .

If the random field is isotropic (invariant under rotations), then isotropy can substantially reduce the computational burden. Indeed, the probability $\mathbb{P}(X_D > u, X_{\mathcal{N}(D)} \leq u)$ depends only on the shape of D up to rigid motions; all rotated or reflected copies of a given shape contribute the same probability and differ only by their multiplicity. For example, under nearest neighbors in \mathbb{Z}^2 , the set $\mathcal{C}_2^{\text{root}}$ consists of two translates of the same shape, while $\mathcal{C}_3^{\text{root}}$ in (2.9) reduces to two geometric types: straight-line shapes and L -shapes. \square

Remark 2.7 [Boundary representation of $\sum_{k \geq 1} w_k$.] Motivated by the one-dimensional formula, we present an alternative representation of $\sum_{k \geq 1} w_k$. Let

$$B = \{t \in \mathcal{N}(o) : t <_{\text{lex}} o\} = \{-e_i : i = 1, \dots, d\}, \quad H = \{t \in \mathbb{Z}^d \setminus \mathcal{N}(o) : t <_{\text{lex}} o\}.$$

Because the root o is the lexicographically smallest point in its cluster, we can write

$$\begin{aligned} \sum_{k=1}^{\infty} w_k &= \mathbb{P}(\text{there exists a cluster above } u \text{ with root at } o) \\ &= \mathbb{P}(X_o > u, X_B \leq u, \text{and there is no exceedance path from } o \text{ to } H) \\ &= \mathbb{P}(X_o > u, X_B \leq u) \\ &\quad - \mathbb{P}(X_o > u, X_B \leq u, \text{and } \exists \text{ exceedance path from } o \text{ to some } t \in H) \end{aligned} \tag{2.14}$$

When $d = 1$, the last probability in (2.14) vanishes (there is no exceedance path from o to -2), so $\sum_{k=1}^{\infty} w_k = \mathbb{P}(X_0 > u, X_{-1} \leq u)$. For $d \geq 2$, this correction term involves all possible long-range exceedance paths and is generally difficult to evaluate explicitly. \square

2.3.3 Clusters containing the origin versus rooted at the origin

For $k = 1, 2, \dots$, define

$$\mathcal{C}_k^{\text{inside}} = \{\text{all size-}k \text{ clusters above } u \text{ that contain the origin } o\}.$$

That is, the origin lies somewhere in the cluster, but is not necessarily the root. For each $D \in \mathcal{C}_k^{\text{root}}$ there are k placements of the origin in D , and therefore

$$|\mathcal{C}_k^{\text{inside}}| = k|\mathcal{C}_k^{\text{root}}|. \tag{2.15}$$

Let w_k^{inside} denote the probability that a size- k cluster above u contains the origin:

$$w_k^{\text{inside}} = \sum_{D \in \mathcal{C}_k^{\text{inside}}} \mathbb{P}(X_D > u, X_{\mathcal{N}(D)} \leq u). \tag{2.16}$$

By stationarity and (2.15), we have

$$w_k^{\text{inside}} = kw_k. \tag{2.17}$$

Combining (2.17) with Theorem 2.3, we obtain immediately the following formula for the cluster size distribution based on w_k^{inside} .

Corollary 2.8. *Under the assumptions of Theorem 2.3,*

$$\mathbb{P}(S_u = k) = \frac{w_k^{\text{inside}}/k}{\sum_{j=1}^{\infty} (w_j^{\text{inside}}/j)}, \quad k = 1, 2, \dots,$$

where w_k^{inside} is defined in (2.16).

2.3.4 Monte-Carlo estimation of w_k for large k

For large cluster sizes the exact probabilities w_k are both analytically intractable and extremely small, which makes direct estimation difficult. In contrast, the quantities $w_k^{\text{inside}} = kw_k$ are larger and thus easier to estimate. Heuristically, by (2.16),

$$w_k^{\text{inside}} \approx \text{average number of size-}k \text{ clusters above } u \text{ that contain the origin } o.$$

This observation leads to a simple Monte-Carlo estimator. Simulate M independent realizations of the random field on a finite window containing the origin. For the m -th realization, let I_m be the indicator that there exists a size- k cluster containing the origin and not touching the boundary of the simulation window (to avoid edge effects). Then

$$\tilde{w}_k^{\text{inside}} = \frac{1}{M} \sum_{m=1}^M I_m$$

is an unbiased estimator of w_k^{inside} . The corresponding *Monte-Carlo estimator* of w_k is

$$\tilde{w}_k = \frac{\tilde{w}_k^{\text{inside}}}{k} = \frac{1}{Mk} \sum_{m=1}^M I_m. \quad (2.18)$$

A refined estimator. Building on this idea, we now introduce a refined Monte-Carlo procedure that extracts more information from each simulated realization. Simulate M independent realizations of the field on a finite domain of size N^d containing the origin (for example, $[-50, 50]^2$ when $d = 2$). Within this domain, select a smaller subdomain of size n^d that also contains the origin (e.g., $[-25, 25]^2$ when $d = 2$).

For a given realization, consider all size- k clusters that intersect the n^d subdomain but do not touch the boundary of the full N^d domain. If a size- k cluster lies entirely inside the subdomain, it is counted as one. If a size- k cluster intersects the subdomain in exactly x lattice points, it is counted with weight x/k . We refer to the quantity x/k as the *intersection proportion*. This definition naturally includes the fully contained case, for which the intersection proportion equals one.

Let J_m denote the total weighted count of size- k clusters in the m -th realization, where each cluster is weighted by its intersection proportion as described above. The *refined Monte-Carlo estimator* of w_k is then

$$\tilde{w}_k = \frac{1}{n^d M} \sum_{m=1}^M J_m. \quad (2.19)$$

The estimator in (2.18) based on w_k^{inside} corresponds to the special case in which the n^d subdomain is reduced to the singleton $\{o\}$, so that $n = 1$. In this setting, a size- k cluster is observed if and only if it contains the origin, and it is counted with weight $1/k$, which coincides with the intersection proportion. Consequently, $J_m = I_m/k$, and the estimator in (2.19) reduces to that in (2.18).

The refined estimator therefore generalizes the origin-based approach by incorporating information from multiple lattice sites within a subdomain of size n^d . As a result, each simulated realization contributes more effectively to the estimation of w_k , leading to improved statistical efficiency, particularly when k is large and w_k is small.

3 The peak-based cluster size distribution

When the random field X_t is nonstationary, the cluster size distribution in (2.1) becomes challenging to analyze. This difficulty arises because, in the nonstationary setting, the conditional probability in (2.1) depends on the spatial location of the observed cluster C_u , as the covariance structure of the field varies across the domain. Consequently, a single global cluster size distribution is generally not well defined. A more appropriate formulation is a local, spatially varying cluster size distribution that reflects the heterogeneity in the covariance structure of the field.

A second motivation comes from the fact that every cluster contains at least one local maximum (typically only a few), which can serve as a natural representative of the cluster. Moreover, for high thresholds u , clusters tend to be dominated by a single prominent peak. Since peak analysis is itself a mature and active area [5, 6, 7, 8, 15, 17], it is natural and valuable to study the peak-based cluster size distribution from both theoretical and applied perspectives. Specifically, given that a local maximum exceeding u is observed at t , we consider the distribution of the size of the cluster containing that peak.

Formally, let $C_u(t)$ denote the cluster above u that contains t , and let $S_u^{\text{peak}}(t)$ be its size, conditional on t being a local maximum above u . The *peak-based cluster size distribution* is defined by

$$\mathbb{P}(S_u^{\text{peak}}(t) = k) = \mathbb{P}(|C_u(t)| = k \mid t \text{ is a local maximum and } X_t > u), \quad k = 1, 2, \dots \quad (3.1)$$

In signal detection problems, one is often interested in peaks that are not only high in amplitude but also substantial in spatial extent. This is particularly relevant in neuroimaging applications, where extended activation patterns are more scientifically interpretable than isolated spikes [10, 20, 23, 25]. A peak-based formulation of the cluster size distribution provides a natural and efficient framework for quantifying such effects and assessing their significance, through p -values, when detecting spatially extended signals.

As in the study of exact cluster size distributions, we first present the one-dimensional case, where the structure of clusters and the corresponding computations admit explicit characterization, and then extend the results to \mathbb{Z}^d .

3.1 Discrete processes on \mathbb{Z}

Let $\{X_t : t \in \mathbb{Z}\}$ be a discrete process on \mathbb{Z} , and fix a threshold $u \in \mathbb{R}$. The excursion set $\{t \in \mathbb{Z} : X_t > u\}$ decomposes into clusters (connected components). Conditional on a local

maximum t with $X_t > u$, the associated cluster $C_u(t)$ consists of all connected exceedance sites connected to t .

For $k = 1$, the cluster $C_u(t)$ is the singleton $\{t\}$, which occurs precisely when both neighbors of t fall below u . Hence

$$\mathbb{P}(S_u^{\text{peak}}(t) = 1) = \mathbb{P}(X_{t-1} \leq u, X_{t+1} \leq u \mid X_t > u, X_t > \max\{X_{t-1}, X_{t+1}\}). \quad (3.2)$$

For $k = 2$, the cluster $C_u(t)$ must be either $\{t, t+1\}$ or $\{t-1, t\}$, so

$$\begin{aligned} \mathbb{P}(S_u^{\text{peak}}(t) = 2) &= \mathbb{P}(X_{t-1} \leq u, X_{t+1} > u, X_{t+2} \leq u \mid X_t > u, X_t > \max\{X_{t-1}, X_{t+1}\}) \\ &\quad + \mathbb{P}(X_{t-2} \leq u, X_{t-1} > u, X_{t+1} \leq u \mid X_t > u, X_t > \max\{X_{t-1}, X_{t+1}\}). \end{aligned} \quad (3.3)$$

If X_t is stationary, then by symmetry the two probabilities on the right side of (3.3) coincide.

More generally, for a size- k cluster containing t , the peak site t partitions the cluster into a left part and a right part. Since t itself exceeds u , the number of exceedance sites to the right of t , denoted $|C_u^{\text{right}}(t)|$, can range from 0 to $k-1$; the number to the left is then $|C_u^{\text{left}}(t)| = k-1 - |C_u^{\text{right}}(t)|$. By (3.1), for $k \geq 1$,

$$\mathbb{P}(S_u^{\text{peak}}(t) = k) = \sum_{j=0}^{k-1} \mathbb{P}(|C_u^{\text{right}}(t)| = j, |C_u^{\text{left}}(t)| = k-1-j \mid t \text{ is local max and } X_t > u).$$

The event $\{|C_u^{\text{right}}(t)| = j, |C_u^{\text{left}}(t)| = k-1-j\}$ is equivalent to

$$X_{t-k+j} \leq u, X_{t-k+j+1} > u, \dots, X_{t+j} > u, X_{t+j+1} \leq u.$$

Therefore,

$$\begin{aligned} &\mathbb{P}(S_u^{\text{peak}}(t) = k) \\ &= \frac{\sum_{j=0}^{k-1} \mathbb{P}(X_{t-k+j} \leq u, X_{t-k+j+1} > u, \dots, X_{t+j} > u, X_{t+j+1} \leq u, X_t > \max\{X_{t-1}, X_{t+1}\})}{\mathbb{P}(X_t > u, X_t > \max\{X_{t-1}, X_{t+1}\})}. \end{aligned} \quad (3.4)$$

In the stationary case, the contributions corresponding to j and $k-1-j$ are equal by symmetry.

Example 3.1 Let $X_t, t \in \mathbb{Z}$, be a white noise process with common continuous CDF F . Let $p = F(u)$ and $q = 1 - p$. Note that, if Y_1, Y_2 and Y_3 are i.i.d. with CDF F and density f , then

$$\mathbb{P}(Y_1 > Y_2, Y_1 > Y_3 \mid Y_1 = x) = \mathbb{P}(Y_2 < x)^2 = F(x)^2,$$

so

$$\mathbb{P}(Y_1 > u, Y_1 > Y_2, Y_1 > Y_3) = \int_u^\infty f(x)F(x)^2 dx = \frac{1 - F(u)^3}{3} = \frac{1 - p^3}{3}.$$

Similarly,

$$\begin{aligned} \mathbb{P}(Y_1 > Y_2 > u) &= \int_u^\infty f(x)(1 - F(x))dx = \frac{(1 - F(u))^2}{2} = \frac{q^2}{2}, \\ \mathbb{P}(Y_1 > Y_2 > u, Y_1 > Y_3 > u) &= \int_u^\infty f(x)(F(x) - F(u))^2 dx = \frac{(1 - F(u))^3}{3} = \frac{q^3}{3}. \end{aligned}$$

It follows from (3.2) and (3.3) that

$$\begin{aligned}\mathbb{P}(S_u^{\text{peak}}(t) = 1) &= \frac{\mathbb{P}(X_{t-1} \leq u, X_t > u, X_{t+1} \leq u)}{\mathbb{P}(X_t > u, X_t > \max\{X_{t-1}, X_{t+1}\})} = \frac{3p^2q}{1-p^3}, \\ \mathbb{P}(S_u^{\text{peak}}(t) = 2) &= \frac{2\mathbb{P}(X_{t-1} \leq u, X_t > X_{t+1} > u, X_{t+2} \leq u)}{\mathbb{P}(X_t > u, X_t > \max\{X_{t-1}, X_{t+1}\})} = \frac{3p^2q^2}{1-p^3}.\end{aligned}$$

Similarly,

$$\begin{aligned}\mathbb{P}(S_u^{\text{peak}}(t) = 3) &= \frac{2\mathbb{P}(X_{t-1} \leq u, X_t > X_{t+1} > u, X_{t+2} > u, X_{t+3} \leq u)}{\mathbb{P}(X_t > u, X_t > \max\{X_{t-1}, X_{t+1}\})} \\ &\quad + \frac{\mathbb{P}(X_{t-2} \leq u, X_t > X_{t-1} > u, X_t > X_{t+1} > u, X_{t+2} \leq u)}{\mathbb{P}(X_t > u, X_t > \max\{X_{t-1}, X_{t+1}\})} \\ &= \frac{p^2q^3 + p^2q^3/3}{(1-p^3)/3} = \frac{4p^2q^3}{1-p^3}.\end{aligned}$$

In general, for all $k \geq 1$, we have

$$\mathbb{P}(S_u^{\text{peak}}(t) = k) = \begin{cases} \frac{3p^2q}{1-p^3}, & k = 1, \\ \frac{(k+1)p^2q^k}{1-p^3}, & k \geq 2. \end{cases} \quad (3.5)$$

This gives the exact peak-based cluster size distribution for the one-dimensional i.i.d. case. \square

3.2 Discrete random fields on \mathbb{Z}^d

Now we consider a random field $\{X_t : t \in \mathbb{Z}^d\}$ on the d -dimensional lattice. For $k \geq 1$ and a fixed site t , define

$$\mathcal{C}_k^{\text{peak}}(t) = \{\text{size-}k \text{ clusters above } u \text{ that contain } t \text{ as a local maximum}\}. \quad (3.6)$$

This is a natural analogue to $\mathcal{C}_k^{\text{inside}}$, with the origin replaced by t . For example, in \mathbb{Z}^2 under nearest neighbors, $\mathcal{C}_1^{\text{peak}}(t) = \{t\}$, $\mathcal{C}_2^{\text{peak}}(t)$ consists of four sets

$$\{t, t + e_1\}, \{t, t - e_1\}, \{t, t + e_2\}, \{t, t - e_2\},$$

and $\mathcal{C}_3^{\text{peak}}(t)$ consists of 18 sets in total. In general,

$$|\mathcal{C}_k^{\text{peak}}(t)| = |\mathcal{C}_k^{\text{inside}}| = k |\mathcal{C}_k^{\text{root}}|,$$

since each rooted cluster of size k has k possible locations for t . Under Moore neighbors, $\mathcal{C}_k^{\text{peak}}(t)$ contains additional shapes; for example, when $k = 2$, it also includes four diagonal pairs that connect t to diagonal neighbors.

Recall that $\mathcal{N}(D)$ in (2.10) denotes the exterior neighbor set of D . We now state the peak-based cluster size distribution on \mathbb{Z}^d .

Theorem 3.2. Let $\{X_t : t \in \mathbb{Z}^d\}$ be a random field on \mathbb{Z}^d and let $u \in \mathbb{R}$ be a fixed threshold. Then, for $k = 1, 2, \dots$,

$$\mathbb{P}(S_u^{\text{peak}}(t) = k) = \frac{w_k^{\text{peak}}(t)}{\mathbb{P}(X_t > u, X_t > \max_{s \in \mathcal{N}(t)} X_s)}, \quad (3.7)$$

where $w_k^{\text{peak}}(t)$ denotes the probability that t is a local maximum above u whose associated cluster has size k , i.e.,

$$w_k^{\text{peak}}(t) = \sum_{D \in \mathcal{C}_k^{\text{peak}}(t)} \mathbb{P}\left(X_D > u, X_{\mathcal{N}(D)} \leq u, X_t > \max_{s \in \mathcal{N}(t)} X_s\right). \quad (3.8)$$

Proof. The conditional event in (3.1) can be written as

$$\mathbb{P}(t \text{ is a local maximum and } X_t > u) = \mathbb{P}\left(X_t > u, X_t > \max_{s \in \mathcal{N}(t)} X_s\right).$$

Given that t is a local maximum above u , the cluster $C_u(t)$ has size k if and only if the set of exceedance sites containing t coincides with one of the shapes in $\mathcal{C}_k^{\text{peak}}(t)$. Thus, by (3.1), for $k = 1, 2, \dots$,

$$\begin{aligned} & \mathbb{P}(S_u^{\text{peak}}(t) = k) \\ &= \sum_{D \in \mathcal{C}_k^{\text{peak}}(t)} \mathbb{P}(X_D > u, X_{\mathcal{N}(D)} \leq u \mid t \text{ is a local maximum and } X_t > u) \\ &= \frac{\sum_{D \in \mathcal{C}_k^{\text{peak}}(t)} \mathbb{P}(X_D > u, X_{\mathcal{N}(D)} \leq u, X_t > \max_{s \in \mathcal{N}(t)} X_s)}{\mathbb{P}(X_t > u, X_t > \max_{s \in \mathcal{N}(t)} X_s)}, \end{aligned}$$

where we have used the fact that $X_D > u$ implies $X_t > u$ since t belongs to all $D \in \mathcal{C}_k^{\text{peak}}(t)$. Identifying the numerator with $w_k^{\text{peak}}(t)$ in (3.8) yields (3.7). \square

Theorem 3.2 holds for general random fields on \mathbb{Z}^d ; no stationarity assumption is required. Moreover, the denominator in (3.7) involves only the joint distribution of $\{X_s : s \in \{t\} \cup \mathcal{N}(t)\}$ and is easy to compute explicitly, making it feasible to obtain closed-form expressions for $\mathbb{P}(S_u^{\text{peak}}(t) = k)$ for moderate k . In contrast, for the exact cluster size distribution (2.11), the normalizing constant $\sum_{j \geq 1} w_j$ generally involves global connectivity effects and often requires numerical approximation.

Example 3.3 Let $X_t, t \in \mathbb{Z}^2$, be a two-dimensional white noise field with common continuous CDF F . Let $p = F(u)$ and $q = 1 - p$. We first consider nearest neighbors. By analyzing the shapes in $\mathcal{C}_k^{\text{peak}}(t)$ and applying arguments similar to Example 3.1, one finds that the denominator in (3.7) equals $(1 - p^5)/5$, and

$$w_1^{\text{peak}}(t) = p^4 q, \quad w_2^{\text{peak}}(t) = 2p^6 q^2, \quad w_3^{\text{peak}}(t) = \frac{8}{3}(2p^7 + p^8)q^3.$$

Taking the ratio yields the following probabilities:

$$\begin{aligned}\mathbb{P}(S_u^{\text{peak}}(t) = 1) &= \frac{5p^4q}{1-p^5}, & \mathbb{P}(S_u^{\text{peak}}(t) = 2) &= \frac{10p^6q^2}{1-p^5}, \\ \mathbb{P}(S_u^{\text{peak}}(t) = 3) &= \frac{40(2p^7 + p^8)q^3}{3(1-p^5)}.\end{aligned}$$

Under Moore neighbors, the denominator in (3.7) is $(1-p^9)/9$, and

$$w_1^{\text{peak}}(t) = p^8q, \quad w_2^{\text{peak}}(t) = 2(p^{10} + p^{12})q^2, \quad w_3^{\text{peak}}(t) = \frac{4}{3}(5p^{12} + 8p^{14} + 4p^{15} + 2p^{16})q^3.$$

Therefore,

$$\begin{aligned}\mathbb{P}(S_u^{\text{peak}}(t) = 1) &= \frac{9p^8q}{1-p^9}, & \mathbb{P}(S_u^{\text{peak}}(t) = 2) &= \frac{18(p^{10} + p^{12})q^2}{1-p^9}, \\ \mathbb{P}(S_u^{\text{peak}}(t) = 3) &= \frac{12(5p^{12} + 8p^{14} + 4p^{15} + 2p^{16})q^3}{1-p^9}.\end{aligned}$$

As k increases, the combinatorial complexity of $\mathcal{C}_k^{\text{peak}}(t)$ grows quickly, so it is difficult to obtain closed-form expressions for $w_k^{\text{peak}}(t)$. Nevertheless, $w_k^{\text{peak}}(t)$ can be evaluated numerically by enumerating cluster shapes or approximated via Monte-Carlo methods. \square

Remark 3.4 [An alternative representation.] By definition (3.8), $\sum_{j \geq 1} w_j^{\text{peak}}(t)$ is the probability that t is a local maximum above u whose associated cluster has some finite size:

$$\sum_{j=1}^{\infty} w_j^{\text{peak}}(t) = \mathbb{P}(t \text{ is a local maximum and } X_t > u).$$

Thus (3.7) can equivalently be written as

$$\mathbb{P}(S_u^{\text{peak}}(t) = k) = \frac{w_k^{\text{peak}}(t)}{\sum_{j=1}^{\infty} w_j^{\text{peak}}(t)}. \quad (3.9)$$

\square

Remark 3.5 [Empirical peak-based distribution for nonstationary fields.] We now verify that (3.7) is consistent with the empirical peak-based cluster size distribution obtained from simulations. Suppose we simulate M independent realizations of the nonstationary random field. For a fixed site t , the empirical probability mass function is

$$\begin{aligned}& \frac{\#\{\text{realizations where } t \text{ is a peak above } u \text{ with associated cluster of size } k\}}{\#\{\text{realizations where } t \text{ is a peak above } u\}} \\ &= \frac{\#\{\text{realizations where } t \text{ is a peak above } u \text{ with associated cluster of size } k\}/M}{\#\{\text{realizations where } t \text{ is a peak above } u\}/M} \\ &\xrightarrow{a.s.} \frac{\mathbb{P}(t \text{ is a peak above } u \text{ with associated cluster of size } k)}{\mathbb{P}(t \text{ is a peak above } u)} \\ &= \frac{w_k^{\text{peak}}(t)}{\sum_{j=1}^{\infty} w_j^{\text{peak}}(t)}, \quad \text{as } M \rightarrow \infty,\end{aligned}$$

where the convergence follows from the strong law of large numbers. Thus, as the number of simulations increases, empirical relative frequencies converge to the theoretical peak-based cluster size distribution. \square

Remark 3.6 [Empirical peak-based distribution for stationary fields.] If the random field X_t is stationary, then $w_k^{\text{peak}}(t)$ and $S_u^{\text{peak}}(t)$ do not depend on t , so we simply write w_k^{peak} and S_u^{peak} . In this case,

$$\mathbb{P}(S_u^{\text{peak}} = k) = \frac{w_k^{\text{peak}}}{\sum_{j=1}^{\infty} w_j^{\text{peak}}}, \quad k = 1, 2, \dots$$

If the observation domain contains N^d lattice points, then $N^d w_k^{\text{peak}}$ is the expected number of local maxima above u whose associated clusters have size k . A natural empirical estimator of w_k^{peak} is

$$\hat{w}_k^{\text{peak}} = \frac{\#\{\text{local maxima above } u \text{ with associated cluster of size } k\}}{N^d}.$$

Similarly, $N^d \sum_{j=1}^{\infty} w_j^{\text{peak}}$ is the expected total number of local maxima above u . Therefore, we have the following empirical relation:

$$\begin{aligned} & \frac{\#\{\text{local maxima above } u \text{ with associated cluster of size } k\}}{\#\{\text{local maxima above } u\}} \\ &= \frac{\#\{\text{local maxima above } u \text{ with associated cluster of size } k\}/N^d}{\#\{\text{local maxima above } u\}/N^d} \\ &= \frac{\hat{w}_k^{\text{peak}}}{\sum_{j=1}^{\infty} \hat{w}_j^{\text{peak}}} \xrightarrow{\text{a.s.}} \frac{w_k^{\text{peak}}}{\sum_{j=1}^{\infty} w_j^{\text{peak}}}, \quad \text{as } N \rightarrow \infty, \end{aligned}$$

where the convergence follows from the strong law of large numbers under stationarity and ergodicity. \square

Remark 3.7 [Monte-Carlo estimation of w_k^{peak} for stationary fields.] For large k , the quantities $w_k^{\text{peak}}(t)$ are typically extremely small and difficult to compute exactly. Direct estimation is usually inefficient, as it would require simulating realizations where the site t is a local maximum above the threshold u , an event that occurs with very low probability. We restrict attention here to stationary random fields, where $w_k^{\text{peak}}(t)$ does not depend on the location t and can be written simply as w_k^{peak} .

We propose a Monte-Carlo estimator analogous to the refined procedure in Section 2.3.4. Simulate M independent realizations of the field on a domain of size N^d , and select an interior subdomain of size n^d . For the m -th realization, let L_m denote the number of local maxima above u that fall within the n^d subdomain, whose associated clusters have size k and do not touch the boundary of the full N^d domain (to avoid boundary effects). Then the *Monte-Carlo estimator* of w_k^{peak} is

$$\tilde{w}_k^{\text{peak}} = \frac{1}{n^d M} \sum_{m=1}^M L_m. \quad (3.10)$$

By aggregating peak events across the n^d interior sites, each realization contributes substantially more information than a single-site estimator, yielding improved statistical efficiency, especially when k is large and w_k^{peak} is small. \square

Remark 3.8 [High thresholds.] When the threshold u is high, then each cluster typically contains a unique local maximum with probability close to one. For a stationary random field and large u , the peak-based and exact cluster size distributions therefore nearly coincide:

$$\mathbb{P}(S_u^{\text{peak}} = k) \approx \mathbb{P}(S_u = k), \quad k = 1, 2, \dots$$

Furthermore, at high thresholds, large clusters are rarely observed, so both w_k and w_k^{peak} are negligible for large k . As a result, the computation of both the exact and peak-based cluster size distributions is substantially simplified. \square

4 Numerical Results and Simulations

We present numerical and simulation results that illustrate the practical performance of the proposed methods for computing the cluster size distribution and the associated quantities w_k . For each example (except the nonstationary case where only peak-based distributions are available), we report both theoretical cluster size distributions, including exact and peak-based formulations, and empirical counterparts obtained from simulated random fields.

As discussed earlier, for general random fields, particularly in dimensions $d \geq 2$, explicit expressions for w_k , w_k^{peak} , $\mathbb{P}(S_u = k)$, and $\mathbb{P}(S_u^{\text{peak}} = k)$ are typically unavailable. Consequently, theoretical values reported below were evaluated numerically or by Monte–Carlo methods except where explicit formulas exist and are indicated.

In the tables below, we report up to the first ten values of w_k and w_k^{peak} , together with their empirical estimates \hat{w}_k and \hat{w}_k^{peak} , all rounded to five decimal places. For completeness, we also report the corresponding partial sums $\sum_{k=1}^{\infty} w_k$, $\sum_{k=1}^{\infty} w_k^{\text{peak}}$, $\sum_{k=1}^{\infty} \hat{w}_k$ and $\sum_{k=1}^{\infty} \hat{w}_k^{\text{peak}}$ over the computed range. Normalizing by these sums yields the cluster size probability mass functions. Specifically, the ratios

$$\frac{w_k}{\sum_{k=1}^{\infty} w_k} = \mathbb{P}(S_u = k), \quad \frac{\hat{w}_k}{\sum_{k=1}^{\infty} \hat{w}_k}, \quad \frac{w_k^{\text{peak}}}{\sum_{k=1}^{\infty} w_k^{\text{peak}}} = \mathbb{P}(S_u^{\text{peak}} = k), \quad \frac{\hat{w}_k^{\text{peak}}}{\sum_{k=1}^{\infty} \hat{w}_k^{\text{peak}}}$$

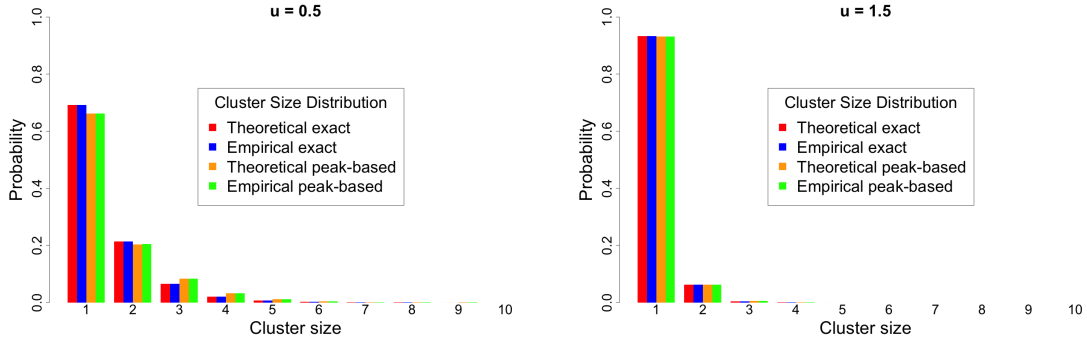
correspond, respectively, to the theoretical and empirical exact cluster size distributions, and to the theoretical and empirical peak-based cluster size distributions. For each example, these distributions are also displayed graphically as histograms to facilitate visual comparison.

4.1 Gaussian processes on \mathbb{Z} .

In one dimension we consider three types of Gaussian processes: (i) Gaussian white noise, (ii) stationary correlated Gaussian processes, and (iii) a nonstationary Gaussian process. Results

Table 1: Gaussian white noise process on \mathbb{Z} .

(a) Theoretical and empirical exact, peak-based cluster size distributions.


 (b) Theoretical and empirical values of w_k , w_k^{peak} and probabilities (in parentheses).

Size k	$w_k \left(\frac{w_k}{\sum w_k} \right)$	$\hat{w}_k \left(\frac{\hat{w}_k}{\sum \hat{w}_k} \right)$	$w_k^{\text{peak}} \left(\frac{w_k^{\text{peak}}}{\sum w_k^{\text{peak}}} \right)$	$\hat{w}_k^{\text{peak}} \left(\frac{\hat{w}_k^{\text{peak}}}{\sum \hat{w}_k^{\text{peak}}} \right)$
$u = 0.5$	1 .14755 (.69100)	.14752 (.69100)	.14800 (.66100)	.14752 (.66100)
	2 .04553 (.21300)	.04551 (.21300)	.04550 (.20400)	.04551 (.20400)
	3 .01402 (.06570)	.01404 (.06580)	.01870 (.08360)	.01404 (.08390)
	4 .00433 (.02030)	.00433 (.02030)	.00723 (.03240)	.00433 (.03240)
	5 .00134 (.00629)	.00134 (.00627)	.00269 (.01200)	.00134 (.01200)
	6 .00041 (.00192)	.00041 (.00193)	.00096 (.00429)	.00041 (.00431)
$\sum_{k=1}^{\infty}$.21337	.21334	.22300	.21334
$u = 1.5$	1 .05820 (.93300)	.05818 (.93300)	.05823 (.93100)	.05818 (.93200)
	2 .00390 (.06250)	.00389 (.06230)	.00390 (.06240)	.00389 (.06220)
	3 .00026 (.00418)	.00026 (.00417)	.00035 (.00559)	.00026 (.00554)
	4 .00002 (.00032)	.00002 (.00028)	.00003 (.00054)	.00002 (.00046)
	$\sum_{k=1}^{\infty}$.06240	.06234	.06251	.06234

are summarized in Tables 1–3. In all experiments we simulated $M_1 = 10,000$ independent realizations of the process on an integer lattice of length $N_1 = 1,500$.

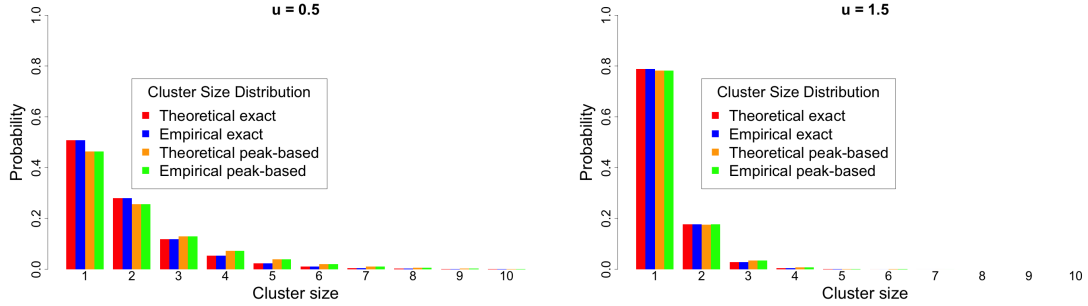
4.1.1 Stationary Gaussian processes on \mathbb{Z}

Let Φ denote the standard normal CDF, and let $p = \Phi(u)$ and $q = 1 - p$. For Gaussian white noise (Example 2.2), the theoretical per-site probabilities are $w_k = p^2 q^k$ for $k \geq 1$, hence $\sum_{k=1}^{\infty} w_k = pq$ and the cluster size distribution is geometric as in (2.3). The peak-based analytic results of Example 3.1 give

$$w_1^{\text{peak}} = p^2 q, \quad w_k^{\text{peak}} = (k+1)p^2 q^k / 3 \text{ for } k \geq 2,$$

Table 2: Gaussian process on \mathbb{Z} with covariance $C(t, s) = e^{-(t-s)^2}$.

(a) Theoretical and empirical exact, peak-based cluster size distributions.



(b) Theoretical and empirical values of w_k , w_k^{peak} and probabilities (in parentheses).

Size k	$w_k \left(\frac{w_k}{\sum w_k} \right)$	$\hat{w}_k \left(\frac{\hat{w}_k}{\sum \hat{w}_k} \right)$	$w_k^{\text{peak}} \left(\frac{w_k^{\text{peak}}}{\sum w_k^{\text{peak}}} \right)$	$\hat{w}_k^{\text{peak}} \left(\frac{\hat{w}_k^{\text{peak}}}{\sum \hat{w}_k^{\text{peak}}} \right)$
$u = 0.5$	1 .08370 (.50800)	.08380 (.50800)	.08370 (.46400)	.08380 (.46400)
	2 .04620 (.28000)	.04620 (.28000)	.04620 (.25600)	.04630 (.25600)
	3 .01950 (.11800)	.01940 (.11800)	.02320 (.12900)	.02320 (.12900)
	4 .00865 (.05250)	.00866 (.05250)	.01310 (.07270)	.01320 (.07290)
	5 .00381 (.02310)	.00379 (.02300)	.00696 (.03860)	.00695 (.03850)
	6 .00168 (.01020)	.00168 (.01020)	.00359 (.01990)	.00361 (.02000)
$\sum_{k=1}^{\infty}$.16500	.18000	.18000
$u = 1.5$	1 .04210 (.78900)	.04210 (.78900)	.04210 (.78100)	.04210 (.78100)
	2 .00947 (.17700)	.00948 (.17800)	.00947 (.17600)	.00949 (.17600)
	3 .00149 (.02800)	.00148 (.02780)	.00181 (.03360)	.00181 (.03350)
	4 .00026 (.00483)	.00026 (.00481)	.00040 (.00740)	.00040 (.00733)
	$\sum_{k=1}^{\infty}$.05340	.05390

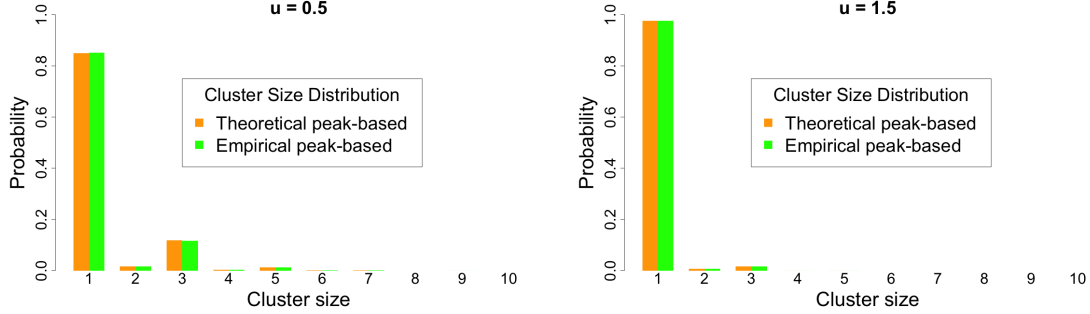
so $\sum_{k=1}^{\infty} w_k^{\text{peak}} = (1 - p^3)/3$ and the peak-based cluster size distribution in (3.5) follows.

For a stationary correlated Gaussian process with covariance $C(t, s) = e^{-(t-s)^2}$, theoretical w_k and $\sum_{k=1}^{\infty} w_k$ were computed from (2.4) and (2.5); theoretical w_k^{peak} and $\sum_{k=1}^{\infty} w_k^{\text{peak}}$ were obtained from the numerator and denominator of (3.4), respectively. The empirical estimators used in simulations are

$$\hat{w}_k = \frac{\#\{\text{size-}k \text{ clusters above } u\}}{M_1 N_1}, \quad \sum_{k=1}^{\infty} \hat{w}_k = \frac{\#\{\text{all clusters above } u\}}{M_1 N_1}, \quad (4.1)$$

Table 3: Nonstationary Gaussian $Y_t = X_t + \cos(\pi t)$, with peak-based inference at $t = 0$.

(a) Theoretical and empirical peak-based cluster size distributions.



(b) Theoretical and empirical values of w_k^{peak} and probabilities (in parentheses).

Size k	$u = 0.5$		$u = 1.5$	
	$w_k^{\text{peak}} \left(\frac{w_k^{\text{peak}}}{\sum w_k^{\text{peak}}} \right)$	$\hat{w}_k^{\text{peak}} \left(\frac{\hat{w}_k^{\text{peak}}}{\sum \hat{w}_k^{\text{peak}}} \right)$	$w_k^{\text{peak}} \left(\frac{w_k^{\text{peak}}}{\sum w_k^{\text{peak}}} \right)$	$\hat{w}_k^{\text{peak}} \left(\frac{\hat{w}_k^{\text{peak}}}{\sum \hat{w}_k^{\text{peak}}} \right)$
1	.57400 (.85000)	.57600 (.85100)	.30000 (.97600)	.30000 (.97600)
2	.01050 (.01550)	.01050 (.01560)	.00232 (.00754)	.00230 (.00750)
3	.07930 (.11700)	.07940 (.11700)	.00493 (.01600)	.00488 (.01590)
4	.00150 (.00222)	.00148 (.00218)	.00004 (.00011)	.00003 (.00011)
5	.00874 (.01290)	.00854 (.01260)	.00006 (.00018)	.00004 (.00015)
$\sum_{k=1}^{\infty}$.67600	.67700	.30700	.30700

and for peak-based quantities

$$\begin{aligned} \hat{w}_k^{\text{peak}} &= \frac{\#\{\text{local maxima above } u \text{ with associated cluster of size } k\}}{M_1 N_1}, \\ \sum_{k=1}^{\infty} \hat{w}_k^{\text{peak}} &= \frac{\#\{\text{local maxima above } u\}}{M_1 N_1}. \end{aligned} \quad (4.2)$$

Tables 1 and 2 report theoretical and empirical values (with normalized probabilities in parentheses) and display histogram comparisons. In both examples the empirical distributions closely match theory. Moreover, as the threshold increases from $u = 0.5$ to $u = 1.5$, the peak-based cluster size distribution approach the exact cluster size distribution, confirming the high-threshold approximation discussed in Remark 3.8.

4.1.2 Nonstationary Gaussian processes on \mathbb{Z}

In the nonstationary setting, only the peak-based cluster size distributions are available, and the peak-based quantities $w_k^{\text{peak}}(t)$ generally depend on the spatial location t . For simplicity, we focus at a fixed reference point $t_0 = 0$, and write $w_k^{\text{peak}}(t_0) = w_k^{\text{peak}}$.

To obtain robust empirical estimates with repeated structure, we increase the number of local maxima that share the same local behavior at 0 by introducing a periodic mean function. Specifically, we consider

$$Y_t = X_t + \cos(\pi t), \quad t \in \mathbb{Z},$$

where X_t is a centered stationary Gaussian process with covariance $C(t, s) = e^{-(t-s)^2}$. Due to stationarity of X_t and periodicity of $\cos(\pi t)$, the local behaviors of Y_t at sites $t \in D_0 = \{0, \pm 2, \pm 4, \dots\}$ (within the simulation domain) are identical. Consequently, the peak-based cluster size distributions coincide at these locations.

Theoretical values of w_k^{peak} and $\sum_{k=1}^{\infty} w_k^{\text{peak}}$ are obtained from the numerator and denominator of (3.4), respectively. Empirical estimators exploit the repeated sites in D_0 :

$$\begin{aligned} \hat{w}_k^{\text{peak}}(t) &= \frac{\#\{\text{local maxima at } t \in D_0 \text{ above } u \text{ with associated cluster of size } k\}}{M_1|D_0|}, \\ \sum_{k=1}^{\infty} \hat{w}_k^{\text{peak}} &= \frac{\#\{\text{local maxima at } t \in D_0 \text{ above } u\}}{M_1|D_0|}, \end{aligned}$$

where, for our experiments, $|D_0| \approx N_1/2$.

Table 3 shows theoretical and empirical values of w_k^{peak} and \hat{w}_k^{peak} , together with normalized probability masses and histogram comparisons. For both threshold levels $u = 0.5$ and $u = 1.5$, the empirical exact peak-based cluster size distributions agree well with theoretical values.

4.2 Gaussian and chi-squared fields on \mathbb{Z}^2 .

On \mathbb{Z}^2 we consider four model classes: (i) stationary correlated Gaussian fields under nearest neighbors, (ii) the same field under Moore neighbors, (iii) Gaussian white noise under Moore neighbors, and (iv) standardized chi-squared fields under Moore neighbors. Results are illustrated in Tables 4–7.

In general, theoretical w_k are computed from (2.12), while theoretical w_k^{peak} and $\sum_{k=1}^{\infty} w_k^{\text{peak}}$ follow from (3.8) and the denominator of (3.7), respectively. For Gaussian white noise (Table 6), these quantities admit closed-form expressions, as derived in Examples 2.4 and 3.3.

Because exact numerical evaluation becomes costly for large cluster sizes, we compute theoretical values exactly for $k \leq 6$ and estimate larger k by Monte–Carlo. Concretely, for $k \geq 7$ we use the refined estimator (2.19) to estimate w_k and $\sum_{k=1}^{\infty} w_k$, and the Monte–Carlo procedure of Remark 3.7 to estimate w_k^{peak} . These Monte–Carlo values were produced from 15,000 independent realizations of the field on a 100×100 integer lattice, with inference restricted to the interior 50×50 subdomain to mitigate boundary bias.

Since simulating correlated random fields on large lattices with a prescribed covariance structure can be computationally demanding, we adopt an alternative strategy to facilitate empirical estimation using multiple moderately sized independent realizations. Specifically, we simulate $M_2 = 2,000$ independent realizations of the field on an integer lattice of size $N_2^2 = 300 \times 300$. The empirical estimators of w_k and $\sum_{k=1}^{\infty} w_k$ are provided in (4.1), with

M_1 and N_1 replaced by M_2 and N_2^2 , respectively. Similarly, the empirical estimators for the peak-based quantities are given by (4.2), with the same substitutions.

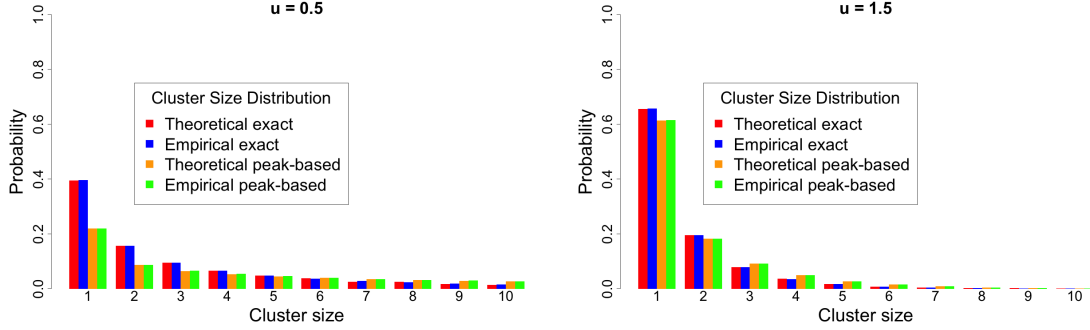
Tables 4 and 5 summarize numerical and simulation results for correlated Gaussian fields on \mathbb{Z}^2 with covariance $C(t, s) = e^{-\|t-s\|^2}$, under nearest and Moore neighbors. The results show that, when moving from nearest to Moore neighbors, as well as from one-dimensional to two-dimensional settings, small clusters occur less frequently while larger clusters become more prevalent. This behavior is a direct consequence of the increased degree of connectivity, which promotes the formation of larger connected components.

In Table 7, the standardized chi-squared field under consideration is $Z_t = (X_t^2 + Y_t^2)/2 - 1$, where X and Y are independent Gaussian fields with covariance $C(t, s) = e^{-\|t-s\|^2}$. Alternatively, one may take X and Y to be independent Gaussian white noise; in this case, the analytic formulas derived in Examples 2.4 and 3.3 apply directly.

Across all four examples presented in Tables 4–7, the empirical exact and peak-based distributions closely match their theoretical counterparts. As the threshold increases from $u = 0.5$ to $u = 1.5$, the peak-based cluster size distribution converges toward the exact distribution, consistent with the high-threshold approximation described in Remark 3.8.

Table 4: Gaussian field on \mathbb{Z}^2 with covariance $C(t, s) = e^{-\|t-s\|^2}$ under nearest neighbors.

(a) Theoretical and empirical exact, peak-based cluster size distributions.

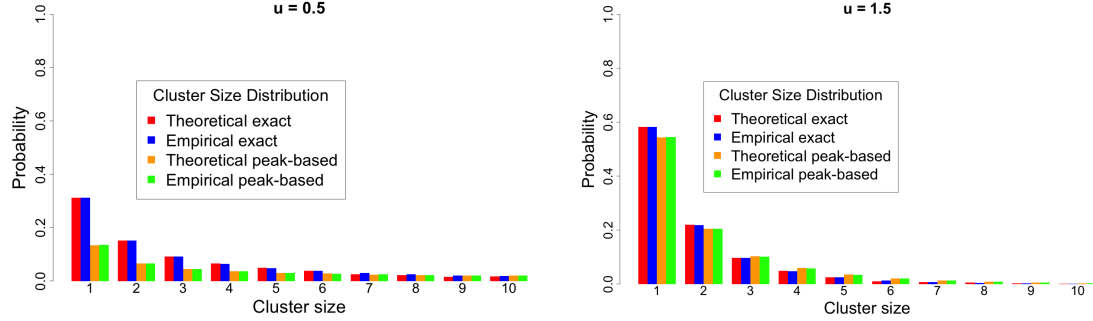


(b) Theoretical and empirical values of w_k , w_k^{peak} and probabilities (in parentheses).

Size k	$w_k \left(\frac{w_k}{\sum w_k} \right)$	$\hat{w}_k \left(\frac{\hat{w}_k}{\sum \hat{w}_k} \right)$	$w_k^{\text{peak}} \left(\frac{w_k^{\text{peak}}}{\sum w_k^{\text{peak}}} \right)$	$\hat{w}_k^{\text{peak}} \left(\frac{\hat{w}_k^{\text{peak}}}{\sum \hat{w}_k^{\text{peak}}} \right)$
$u = 0.5$	1 .02463 (.39536)	.02460 (.39600)	.02463 (.22015)	.02469 (.22000)
	2 .00974 (.15638)	.00971 (.15600)	.00974 (.08710)	.00976 (.08710)
	3 .00592 (.09501)	.00588 (.09430)	.00723 (.06463)	.00731 (.06520)
	4 .00414 (.06651)	.00410 (.06580)	.00596 (.05331)	.00603 (.05380)
	5 .00304 (.04874)	.00299 (.04800)	.00506 (.04524)	.00511 (.04560)
	6 .00233 (.03744)	.00229 (.03680)	.00437 (.03906)	.00451 (.04030)
	7 .00161 (.02591)	.00181 (.02910)	.00398 (.03557)	.00400 (.03570)
	8 .00160 (.02568)	.00146 (.02340)	.00359 (.03208)	.00360 (.03210)
	9 .00110 (.01765)	.00121 (.01940)	.00322 (.02877)	.00329 (.02930)
	10 .00085 (.01364)	.00100 (.01610)	.00298 (.02662)	.00301 (.02680)
$\sum_{k=1}^{\infty}$.06254	.06230	.11188	.11203
$u = 1.5$	1 .02686 (.65523)	.02647 (.65765)	.02686 (.61413)	.02689 (.61474)
	2 .00800 (.19513)	.00785 (.19506)	.00800 (.18288)	.00802 (.18306)
	3 .00325 (.07930)	.00317 (.07868)	.00401 (.09177)	.00401 (.09158)
	4 .00148 (.03610)	.00144 (.03569)	.00216 (.04946)	.00216 (.04925)
	5 .00069 (.01687)	.00067 (.01658)	.00118 (.02696)	.00117 (.02678)
	6 .00034 (.00821)	.00033 (.00809)	.00066 (.01507)	.00066 (.01506)
	7 .00014 (.00348)	.00016 (.00400)	.00037 (.00842)	.00036 (.00843)
	8 .00010 (.00244)	.00008 (.00202)	.00021 (.00480)	.00020 (.00473)
	9 .00008 (.00190)	.00004 (.00105)	.00012 (.00270)	.00012 (.00257)
	$\sum_{k=1}^{\infty}$.04099	.04024	.04374

Table 5: Gaussian field on \mathbb{Z}^2 with covariance $C(t, s) = e^{-\|t-s\|^2}$ under Moore neighbors.

(a) Theoretical and empirical exact, peak-based cluster size distributions.

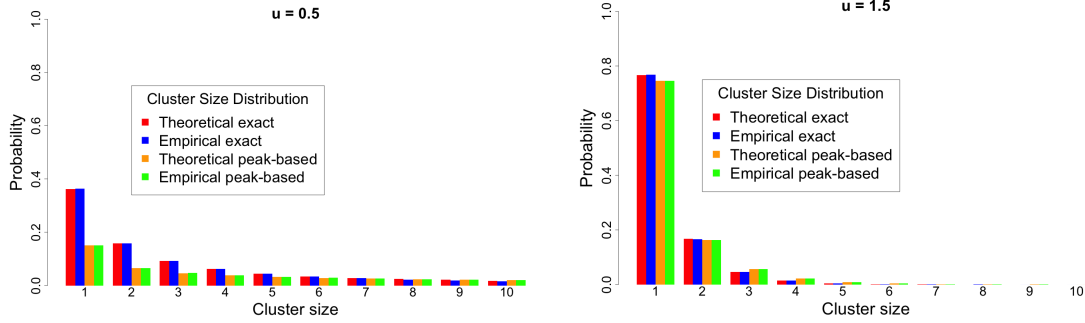


(b) Theoretical and empirical values of w_k , w_k^{peak} and probabilities (in parentheses).

Size k	$w_k \left(\frac{w_k}{\sum w_k} \right)$	$\hat{w}_k \left(\frac{\hat{w}_k}{\sum \hat{w}_k} \right)$	$w_k^{\text{peak}} \left(\frac{w_k^{\text{peak}}}{\sum w_k^{\text{peak}}} \right)$	$\hat{w}_k^{\text{peak}} \left(\frac{\hat{w}_k^{\text{peak}}}{\sum \hat{w}_k^{\text{peak}}} \right)$
$u = 0.5$	1 .01053 (.31200)	.01053 (.31138)	.01052 (.13466)	.01053 (.13463)
	2 .00509 (.15100)	.00511 (.15127)	.00509 (.06557)	.00511 (.06539)
	3 .00307 (.09090)	.00310 (.09170)	.00342 (.04458)	.00345 (.04414)
	4 .00219 (.06480)	.00222 (.06552)	.00277 (.03649)	.00280 (.03583)
	5 .00162 (.04790)	.00165 (.04880)	.00233 (.03080)	.00237 (.03029)
	6 .00127 (.03760)	.00130 (.03834)	.00205 (.02742)	.00229 (.02925)
	7 .00103 (.03040)	.00086 (.02535)	.00186 (.02471)	.00190 (.02434)
	8 .00085 (.02520)	.00073 (.02144)	.00170 (.02281)	.00175 (.02238)
	9 .00072 (.02120)	.00054 (.01610)	.00157 (.02115)	.00161 (.02054)
	10 .00062 (.01820)	.00059 (.01745)	.00146 (.01988)	.00153 (.01961)
$\sum_{k=1}^{\infty}$.03371	.03381	.07389	.07822
$u = 1.5$	1 .02095 (.58301)	.02100 (.58301)	.02095 (.54407)	.02090 (.54407)
	2 .00788 (.21939)	.00785 (.21800)	.00788 (.20468)	.00790 (.20500)
	3 .00350 (.09742)	.00346 (.09630)	.00393 (.10208)	.00392 (.10200)
	4 .00175 (.04867)	.00173 (.04800)	.00226 (.05862)	.00224 (.05820)
	5 .00090 (.02511)	.00089 (.02460)	.00134 (.03478)	.00132 (.03440)
	6 .00033 (.00928)	.00048 (.01320)	.00081 (.02108)	.00081 (.02110)
	7 .00026 (.00716)	.00026 (.00721)	.00049 (.01285)	.00051 (.01320)
	8 .00018 (.00487)	.00015 (.00405)	.00032 (.00823)	.00031 (.00806)
	9 .00007 (.00206)	.00008 (.00227)	.00020 (.00508)	.00019 (.00498)
	10 .00005 (.00130)	.00005 (.00130)	.00012 (.00305)	.00012 (.00306)
$\sum_{k=1}^{\infty}$.03590	.03600	.03850	.03850

Table 6: Gaussian white noise field on \mathbb{Z}^2 under Moore neighbors.

(a) Theoretical and empirical exact, peak-based cluster size distributions.

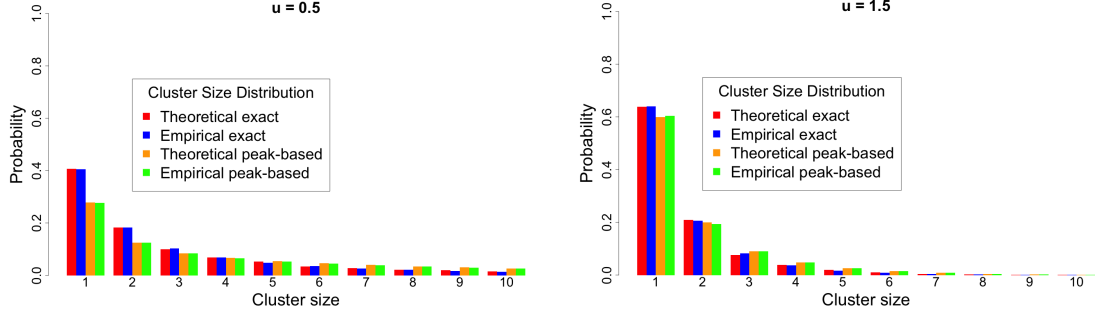


(b) Theoretical and empirical values of w_k , w_k^{peak} and probabilities (in parentheses).

Size k	$w_k \left(\frac{w_k}{\sum w_k} \right)$	$\hat{w}_k \left(\frac{\hat{w}_k}{\sum \hat{w}_k} \right)$	$w_k^{\text{peak}} \left(\frac{w_k^{\text{peak}}}{\sum w_k^{\text{peak}}} \right)$	$\hat{w}_k^{\text{peak}} \left(\frac{\hat{w}_k^{\text{peak}}}{\sum \hat{w}_k^{\text{peak}}} \right)$
$u = 0.5$	1 .01610 (.36300)	.01610 (.36300)	.01612 (.15055)	.01610 (.15100)
	2 .00703 (.15816)	.00703 (.15800)	.00703 (.06565)	.00704 (.06570)
	3 .00407 (.09159)	.00409 (.09210)	.00496 (.04632)	.00499 (.04660)
	4 .00274 (.06162)	.00275 (.06200)	.00404 (.03773)	.00407 (.03800)
	5 .00199 (.04477)	.00200 (.04510)	.00347 (.03237)	.00349 (.03260)
	6 .00152 (.03425)	.00153 (.03440)	.00306 (.02861)	.00308 (.02880)
	7 .00121 (.02718)	.00122 (.02740)	.00278 (.02597)	.00279 (.02600)
	8 .00114 (.02559)	.00098 (.02220)	.00253 (.02360)	.00252 (.02360)
	9 .00094 (.02124)	.00082 (.01840)	.00234 (.02183)	.00231 (.02160)
	10 .00076 (.01710)	.00070 (.01570)	.00214 (.01996)	.00216 (.02020)
$\sum_{k=1}^{\infty}$.04446	.04432	.10502	.10707
$u = 1.5$	1 .03840 (.76645)	.03850 (.76600)	.03842 (.74643)	.03850 (.74600)
	2 .00836 (.16685)	.00837 (.16700)	.00836 (.16249)	.00837 (.16200)
	3 .00231 (.04601)	.00232 (.04620)	.00290 (.05637)	.00291 (.05650)
	4 .00071 (.01407)	.00070 (.01400)	.00109 (.02123)	.00109 (.02120)
	5 .00023 (.00456)	.00023 (.00452)	.00042 (.00819)	.00042 (.00813)
	6 .00008 (.00153)	.00008 (.00151)	.00016 (.00320)	.00016 (.00316)
	7 .00003 (.00053)	.00003 (.00055)	.00006 (.00125)	.00007 (.00129)
	8 .00000 (.00000)	.00001 (.00018)	.00003 (.00051)	.00002 (.00048)
	9 .00000 (.00000)	.00000 (.00007)	.00001 (.00021)	.00001 (.00022)
	10 .00000 (.00000)	.00000 (.00002)	.00001 (.00011)	.00000 (.00007)
$\sum_{k=1}^{\infty}$.05013	.05018	.05148	.05152

Table 7: Standardized chi-squared field on \mathbb{Z}^2 under Moore neighbors.

(a) Theoretical and empirical exact, peak-based cluster size distributions.



(b) Theoretical and empirical values of w_k , w_k^{peak} and probabilities (in parentheses).

Size k	$w_k \left(\frac{w_k}{\sum w_k} \right)$	$\hat{w}_k \left(\frac{\hat{w}_k}{\sum \hat{w}_k} \right)$	$w_k^{\text{peak}} \left(\frac{w_k^{\text{peak}}}{\sum w_k^{\text{peak}}} \right)$	$\hat{w}_k^{\text{peak}} \left(\frac{\hat{w}_k^{\text{peak}}}{\sum \hat{w}_k^{\text{peak}}} \right)$
$u = 0.5$	1 .02497 (.40657)	.02445 (.40512)	.02497 (.27859)	.02445 (.27740)
	2 .01119 (.18226)	.01100 (.18224)	.01113 (.12424)	.01100 (.12479)
	3 .00613 (.09988)	.00625 (.10352)	.00755 (.08422)	.00735 (.08343)
	4 .00423 (.06880)	.00413 (.06845)	.00592 (.06604)	.00577 (.06546)
	5 .00322 (.05244)	.00289 (.04789)	.00487 (.05436)	.00471 (.05339)
	6 .00207 (.03365)	.00212 (.03519)	.00410 (.04570)	.00397 (.04506)
	7 .00169 (.02745)	.00160 (.02658)	.00353 (.03943)	.00339 (.03850)
	8 .00135 (.02198)	.00124 (.02058)	.00307 (.03430)	.00293 (.03327)
	9 .00119 (.01936)	.00098 (.01621)	.00270 (.03011)	.00255 (.02890)
	10 .00094 (.01531)	.00078 (.01295)	.00235 (.02627)	.00223 (.02530)
$\sum_{k=1}^{\infty}$.06141	.05940	.08962	.08638
$u = 1.5$	1 .03164 (.63945)	.03110 (.64100)	.03164 (.60003)	.03110 (.60400)
	2 .01037 (.20958)	.01000 (.20600)	.01057 (.20052)	.01000 (.19400)
	3 .00373 (.07544)	.00397 (.08180)	.00477 (.09049)	.00464 (.09000)
	4 .00193 (.03890)	.00178 (.03680)	.00254 (.04820)	.00247 (.04790)
	5 .00094 (.01900)	.00083 (.01720)	.00138 (.02609)	.00135 (.02610)
	6 .00050 (.01010)	.00041 (.00838)	.00080 (.01516)	.00075 (.01460)
	7 .00019 (.00375)	.00020 (.00413)	.00044 (.00834)	.00042 (.00816)
	8 .00009 (.00177)	.00010 (.00214)	.00025 (.00468)	.00024 (.00469)
	9 .00003 (.00067)	.00005 (.00109)	.00014 (.00270)	.00014 (.00265)
	10 .00004 (.00081)	.00003 (.00057)	.00009 (.00164)	.00008 (.00150)
$\sum_{k=1}^{\infty}$.04950	.04850	.05274	.05130

Acknowledgments

The authors were supported by NSF Grant DMS-2220523 and Simons Foundation Collaboration Grant #854127. We thank Prof. Guofeng Cao and Yu Zhou from the Department of Geography at University of Colorado Boulder for motivating this research topic.

References

- [1] Adler, R. J. (1981). *The Geometry of Random Fields*. Wiley, New York.
- [2] Adler, R. J. and Taylor, J. E. (2007). *Random Fields and Geometry*. Springer, New York.
- [3] Bansal, R. and Peterson, B. S. (2018). Cluster-level statistical inference in fMRI datasets: The unexpected behavior of random fields in high dimensions. *Magn Reson Imaging*, **49**, 101–115.
- [4] Bardeen, J. M., Bond, J. R., Kaiser, N. and Szalay A. S. (1985). The statistics of peaks of Gaussian random fields. *Astrophys. J.*, **304**, 15–61.
- [5] Cheng, D., Cammarota, V., Fantaye, Y., Marinucci, D. and Schwartzman, A. (2020). Multiple testing of local maxima for detection of peaks on the (celestial) sphere. *Bernoulli*, **26**, 31–60.
- [6] Cheng, D. and Schwartzman, A. (2015). Distribution of the height of local maxima of Gaussian random fields. *Extremes*, **18**, 213–240.
- [7] Cheng, D. and Schwartzman, A. (2018). Expected number and height distribution of critical points of smooth isotropic Gaussian random fields. *Bernoulli*, **24**, 3422–3446.
- [8] Cheng, D. and Schwartzman, A. (2017). Multiple testing of local maxima for detection of peaks in random fields. *Ann. Stat.*, **45**, 529–556.
- [9] Chiles, J.-P. and Delfiner, P. (2012). *Geostatistics: Modeling Spatial Uncertainty*. Wiley, New York.
- [10] Chumbley, J. R., Worsley, K., Flandin, G. and Friston, K. J. (2010). Topological FDR for neuroimaging. *Neuroimage*, **49**, 3057–3064.
- [11] Cooley, D., Nychka, D. and Naveau, P. (2007). Bayesian spatial modeling of extreme precipitation return levels. *J. Am. Statist. Assoc.*, **102**, 824–840.
- [12] Cramér, H. and Leadbetter, M. R. (1967). *Stationary and Related Stochastic Processes: Sample Function Properties and Their Applications*. Wiley, New York.
- [13] Davison, A. C., Padoan, S. A. and Ribatet, M. (2012). Statistical modeling of spatial extremes. *Statistical Science*, **27**, 161–168.
- [14] Friston, K. J., Worsley, K. J., Frackowiak, R. S., Mazziotta, J. C. and Evans, A. C. (1994). Assessing the significance of focal activations using their spatial extent. *Human Brain Mapping*, **1**(3), 210–20.
- [15] de Fondeville, R. and Davison, A. C. (2018). High-dimensional peaks-over-threshold inference. *Biometrika*, **105**, 575–592.

[16] Goeman, J. J., Gorecki, P., Monajemi, R., Chen, X., Nichols, T. E. and Weeda, W. (2023). Cluster extent inference revisited: quantification and localisation of brain activity. *Journal of the Royal Statistical Society Series B*, **85**, 1128–1153.

[17] Huser, R. and Davison, A. C. (2014). Space–time modelling of extreme events. *JRSSB*, **76**, 439–461.

[18] Lindgren, G. (1982). Wave characteristics distributions for Gaussian waves – wave-length, amplitude and steepness. *Ocean Engng.*, **9**, 411–432.

[19] Marinucci, D. and Peccati, G. (2011). *Random Fields on the Sphere. Representation, Limit Theorems and Cosmological Applications*. Cambridge University Press.

[20] Poline, J. B., Worsley, K. J., Evans, A. C. and Friston, K. J. (1997). Combining spatial extent and peak intensity to test for activations in functional imaging. *Neuroimage*, **5**, 83–96.

[21] Vanmercke, E. (2010). *Random Fields: Analysis and Synthesis*. World Scientific.

[22] Tan, X., Wu, X., and Liu, B. (2021). Global changes in the spatial extents of precipitation extremes. *Environmental Research Letters*, **16**, 054017.

[23] Worsley, K. J., Marrett, S., Neelin, P., Vandal, A. C., Friston, K. J. and Evans, A. C. (1996). A unified statistical approach for determining significant signals in images of cerebral activation. *Human Brain Mapping*, **4**, 58–73.

[24] Taylor, J. E. and Worsley, K. J. (2007). Detecting sparse signals in random fields, with an application to brain mapping. *J. Am. Statist. Assoc.*, **102**, 913–928.

[25] Zhang, H., Nichols, T. E. and Johnson, T. D. (2009). Cluster mass inference via random field theory. *Neuroimage*, **44**, 51–61.

[26] Zhong, P., Brunner, M., Opitz, T. and Huser, R. (2025). Spatial modeling and future projection of extreme precipitation extents. *Journal of the American Statistical Association*, **120**, 80–95.

DAN CHENG AND JOHN GINOS
 School of Mathematical and Statistical Sciences
 Arizona State University
 900 S. Palm Walk
 Tempe, AZ 85281, U.S.A.
 E-mails: chengdan@gmail.com; jginos@asu.edu